Fully Coupled Body Force–Engine Performance Methodology for Boundary Layer Ingestion

Luis López de Vega,* Guillaume Dufour,† and Nicolás García Rosa†
University of Toulouse, 31055 Toulouse, France

https://doi.org/10.2514/1.B37743

Because of their potential reductions of fuel consumption, disruptive propulsion concepts such as boundary layer ingestion have lately earned the attention of the aerospace community. Because of the increased level of interactions brought by the tight airframe–propulsor integration, an accurate assessment of this benefit requires a detailed study of the engine behavior from both an aerodynamics and an overall performance standpoint. In this context, this Paper presents a fully coupled methodology that integrates a zero-dimensional thermodynamic cycle analysis of the core and a three-dimensional body force representation of the fan stage into a single numerical computation. This approach allows the efficient simulation of fan–distortion interactions and engine overall performance in terms of accuracy vs computational cost tradeoff, making it well suited for conducting full aircraft–engine computational fluid dynamics calculations. The coupling is demonstrated in the assessment of boundary layer ingestion impacts on the small DGEN380 turbofan. Results provide a quantification of such impacts on fan efficiency, engine power demand, thrust specific fuel consumption, flow distortion transfer, and fan stage aeromechanical response, for different engine net thrust settings.

Nomenclature

A	=	surface
a	=	speed of sound
b	=	metal blockage
c_p	=	specifit heat capacity
e	=	specific internal energy
F_{IP}	=	in-plane force
F_n	=	net thrust
f_p^c	=	parallel force source term
f_θ	=	circumferential force source term
$\boldsymbol{f}$	=	force source term
h	=	altitude
h_t	=	specific total enthalpy
K_p	=	nondimensional total pressure coefficient
K_q	=	nondimensional total temperature coefficient
$\mathcal{L}$	=	core source term zone characteristic length
LHV	=	fuel lower heating value
M	=	Mach number
N	=	spool speed
OGV	=	outlet guide vane
P	=	mechanical power
p	=	static pressure
O	=	numerical scheme order
p_t	=	total pressure
Q	=	total temperature source term
r	=	radius
s	=	mesh cell size
T	=	static temperature
T_t	=	total temperature
V	=	velocity magnitude
$\boldsymbol{V}$	=	velocity vector
W	=	mass flow
W_F	=	fuel mass flow
y^+	=	nondimensional wall distance
γ	=	specific heat ratio
ΔT_{ISA}	=	ISA temperature offset
δ	=	numerical error
η	=	isentropic efficiency
π	=	total pressure ratio
τ	=	spool torque
Ω	=	source term zone volume

Subscripts

c	=	corrected
est	=	estimated
L	=	low speed
nom	=	nominal
obs	=	observed
ovr	=	overall
prop	=	propulsive
th	=	thermal
0	=	boundary layer upstream conditions
2	=	fan inlet face
7	=	core nozzle inlet
8	=	core nozzle outlet
13	=	bypass duct
18	=	bypass nozzle outlet
21	=	core inlet
∞	=	flight conditions

Superscipt

$*$	=	target value

I. Introduction

THE economic and environmental constraints imposed to the civil aviation market have made fuel burn reduction a major concern in the design of new aircraft. In this context, emerging propulsion concepts such as boundary layer ingestion (BLI) are being considered as a means to achieve this target. In a BLI configuration, the engines are embedded into the airframe, ingesting boundary layer low-momentum fluid and homogenizing the aircraft wake. These effects decrease the propulsive power requirement and the thrust specific fuel consumption with respect to a podded-engine configuration [1–5]. However, predicting the gains of this disruptive architecture is a complex task, as it requires accounting for overall engine performance, fan response to

*Ph.D. Student, ISAE-SUPAERO, Department of Aerodynamics, Energetics and Propulsion, 10 Avenue Edouard Bélin; currently Flight Physics Capabilities Engineer, Airbus; luis.lopez-de-vega@isae-supaero.fr.

†Associate Professor, ISAE-SUPAERO, Department of Aerodynamics, Energetics and Propulsion.

inlet distortion, aircraft external aerodynamics, and the coupling existing between these disciplines.

Many contributions have considered the assessment of BLI effects. From a system-level perspective, thermodynamic cycle models have been applied to identify key impacts on power plant and aircraft performance [6–9], but the detailed fan aerodynamic response to inflow distortion was not modeled. From the aerodynamics standpoint, boundary layer ingesting fans have received a lot of attention, with various levels of fidelity. Using full-annulus Unsteady Reynolds-Averaged Navier Stokes (URANS) simulations, Fidalgo et al. [10] and Gunn and Hall [11] provided a description of the flow mechanisms of fan–distortion interaction. Lower-fidelity modeling approaches, such as actuator disk methods [1,12,13] and particularly body force models [14–16], have shown a good accuracy in reproducing the main features of distortion transfer and overall impact on fan performance. However, none of the mentioned contributions actually examines the coupling between fan aerodynamics and engine performance.

In the literature, a method that couples aerodynamic and engine performance analysis is the so-called zooming approach, mainly aimed at improving the accuracy of individual component representation in overall performance models. This improvement is achieved through computational fluid dynamics (CFD) calculations of specific engine components, which can range from one-dimensional mean line calculations [17,18] to three-dimensional (3D) CFD simulations [19]. In these contributions, CFD data are used to rescale component maps in the performance model, thus enhancing the predictions over a specific engine operation range. Extending the zooming concept, approaches where the component performance map is fully replaced by a concurrently run CFD simulation have also been proposed by Pachidis et al. [20,21]. In the particular case of fan component modeling, 3D single-passage mixing-plane computations of the fan stage were used by Pilet et al. [22] to study subidle engine operation. Nevertheless, none of these approaches is suited for BLI studies, as their application in the framework of aircraft–engine integration is not straightforward and full-annulus simulations are required to account for distortion transfer.

In this context, the present Paper aims at proposing a methodology that 1) fully couples the fan aerodynamics and the engine performance modeling; 2) is suited for integrated aircraft–engine studies, such as BLI configurations; and 3) is computationally affordable and can be applied in daily design loops. To this end, a PROOSIS-based [23] engine core performance model and a CFD computation of the engine aerodynamics are fully coupled. The simulation of the 3D fan stage aerodynamics is achieved through a body force modeling approach, providing an accuracy comparable to full-annulus URANS simulations, but at a fraction of their computational cost [14,15,24]. To make the approach suited for integrated studies, a simple source term model is proposed to represent the core, thus allowing the flow exhausting from both the core and bypass nozzles to be naturally accounted for in the CFD calculation. From the user standpoint, the overall simulation is driven by specifying one engine performance parameter, such as thrust or fuel mass flow. This approach is implemented in the FlowSimulator environment [25] and completely automates all the information exchanges between the aerodynamic and performance models. The methodology is demonstrated in the assessment of BLI effects on a small turbofan aeropropulsive performance.

The Paper is organized as follows. Section II describes the test case, the models, the algorithm, the implementation, and the metrics of the coupling methodology. Section III presents a verification of the coupling against a thermodynamic cycle calculation for nominal engine operation. In Sec. IV, the effects of BLI are assessed in terms of overall engine performance, fan stage aerodynamics, and rotordynamics. Conclusions and perspectives are discussed in Sec. V.

II. Methodology

The present approach relies on coupling a CFD simulation and an engine performance model. The engine inflow, the fan stage, and the bypass nozzle are simulated by a full-annulus body force approach. The core flow of the engine is represented by a simple source term model, followed by the exhaust core nozzle. The body force model is derived from the blade row geometry and calibrated using reference CFD results, and the model input (the rotational speed) is transferred from the performance model simulation. The source terms of the core model are set to match the thermodynamic variations calculated by the performance model. In the latter, the engine inflow and fan stage are replaced by averaged CFD data. The CFD computation and the engine models are sequentially run and exchange information until convergence is reached. This section first presents the test case used, the DGEN380 turbofan. Then, the different models are described, as are the implementation of the coupling algorithm and the definition of the engine performance metrics considered in this Paper.

A. DGEN380 Turbofan

The DGEN380 is a small turbofan initially developed by Price Induction, now AKIRA Technologies, and is designed to propel four- to five-seat very light jets at a cruise altitude of 10,000 ft and Mach number of 0.35. This engine features a two-spool, unmixed flow architecture. The 14 in. fan stage has 14 rotor blades and 40 outlet guide vanes (OGVs). The engine core comprises a centrifugal compressor driven by a single-stage high-pressure turbine, a reverse-flow combustion chamber, and a single-stage low-pressure turbine driving the fan through a gearbox. The station nomenclature is depicted in Fig. 1, and the performance specifications are displayed in Table 1. A fully instrumented version of this engine is available at the ISAE-SUPAERO turbofan test facility, which has been the focus of several studies including windmilling [26] and transient operation [27]. In this context, the DGEN380 provides a relevant test case to assess the benefits of BLI, as the computational results can potentially be validated using experimental data.

B. Performance Model

Engine performance is modeled through a zero-dimensional (0D) thermodynamic cycle calculation of the core section. The gas turbine simulation tool PROOSIS [23] is used for this purpose. In the context of a CFD–engine performance coupling, the main advantage of PROOSIS lies in its capability to generate standalone applications, known as decks, which can be run outside the original software environment. Turbomachinery components are represented through characteristic maps, and their operation must satisfy basic aerothermodynamic principles: continuity of the mass flow across the different engine stations

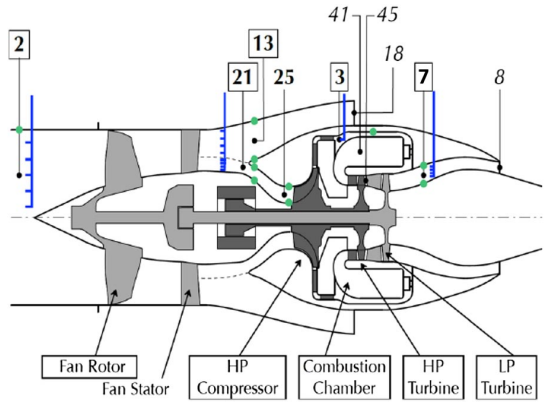

Fig. 1 Meridional view and station nomenclature of the DGEN380 turbofan.

Table 1 DGEN turbofan characteristics

Design point	h = 10,000 ft, M = 0.25
Corrected mass flow, kg/s	12.0 kg/s
BPR	6.5
FPR	1.15
OPR	4.25
T_{t41}	1200 K
Diameter	0.352 m
F_n	1050 N

and power balance on the two engine shafts. The resolution of the resulting system of equations is performed for specified boundary conditions: the flight point and the fuel mass flow. The establishment of the performance maps of each component is detailed in the following.

The 0D fan map is generated from isolated body force calculations of the fan stage, whose modeling accuracy is discussed in Sec. II.D.3. Existing mixing-plane CFD results are used for the generation of the high-pressure compressor map. For the turbines, the map scaling capability of PROOSIS is used to linearly scale a generic component map [28] in order to match the design point values of mass flow, total pressure ratio, and efficiency furnished by the engine manufacturer. All the maps of the performance model are represented using a BETA-type parameterization [29] for interpolation purposes during off-design calculations.

As depicted in Fig. 2, the core model of the DGEN turbofan is derived from the whole engine model and gathers all components from stations 21 to 8, namely, the high-pressure compressor, the combustion chamber, the high- and low-pressure turbines, the primary nozzle, the high- and low-pressure spools, and the gearbox. Furthermore, nozzle aerodynamic coefficients are derived from CFD computations and included in the performance model. To drive the simulation, the user only specifies the fuel mass flow W_F. The outlet static pressure p_8 is derived from the flight conditions and the nozzle total-to-static pressure ratio.

In terms of information exchange in the coupled approach, 1) the total conditions at station 21 p_{t21}, T_{t21} and the torque applied to the low-pressure spool τ_L are retrieved from the fan stage flow simulation, and 2) the fan rotational speed N_L and the total conditions at station 7 p_{t7}, T_{t7} from the engine model are transferred to the global CFD simulation to update the aerodynamic models.

C. Aerodynamic Models

Engine internal aerodynamics are accounted for using a source term modeling approach rather than actually meshing the blade rows. In turbomachinery applications, this technique is known as body force modeling and greatly reduces the computational cost of simulations due to a reduced number of mesh cells and the possibility to handle distorted inflow cases with a steady approach, while providing an accuracy comparable to full-annulus URANS simulations [14]. Body force modeling is applied in the fan stage, whereas a simple source term model is used in the core section.

A meridional view of the aerodynamic model is depicted in Fig. 3. It includes the inlet duct, spinner, rotor and OGV swept volumes, and the core and bypass nozzle outlet sections, which are sized according to their actual values. As no detailed representation of the core aerodynamics is sought, the contours defined between stations 21 and 7 and the position of the core model zone are arbitrary.

1. *Fan Stage Body Force Modeling*

The key idea of body force modeling is to replace the rotor and OGV rows by a volume source field that is active in the region swept by the blades and reacts to local flow conditions, providing the same flow turning and entropy rise as the actual blades. In this contribution, the lift/drag model of Thollet et al. [14] is applied to the fan stage. The model calibration coefficients are obtained from a single-passage, mixing-plane computation at the design operating point. Once the body force model is calibrated, the computation of the volume source field only requires specifying the fan rotational speed N_L, which is retrieved from the core thermodynamic cycle calculation.

2. *Core Source Term Modeling*

Engine core aerodynamic effects are modeled as a total pressure and total temperature rise between stations 21 and 7. For this purpose, a source term model inspired by the body force technique is proposed. This model locally computes the source terms required to reach homogeneous values of total pressure and total temperature at the core nozzle inlet (station 7) and accounts for the mass flow addition due to fuel injection in the combustion chamber. The model inputs (p^*_{t7}, T^*_{t7}, and W_F) are provided by the 0D thermodynamic cycle calculation.

The fundamental motivation of the source term model is to provide an alternative to explicitly imposing the core inlet mass flow through a boundary condition. In fact, the latter approach leads to longer transients because the CFD solver requires iteratively updating the static pressure to match the prescribed value of the mass flow. Moreover,

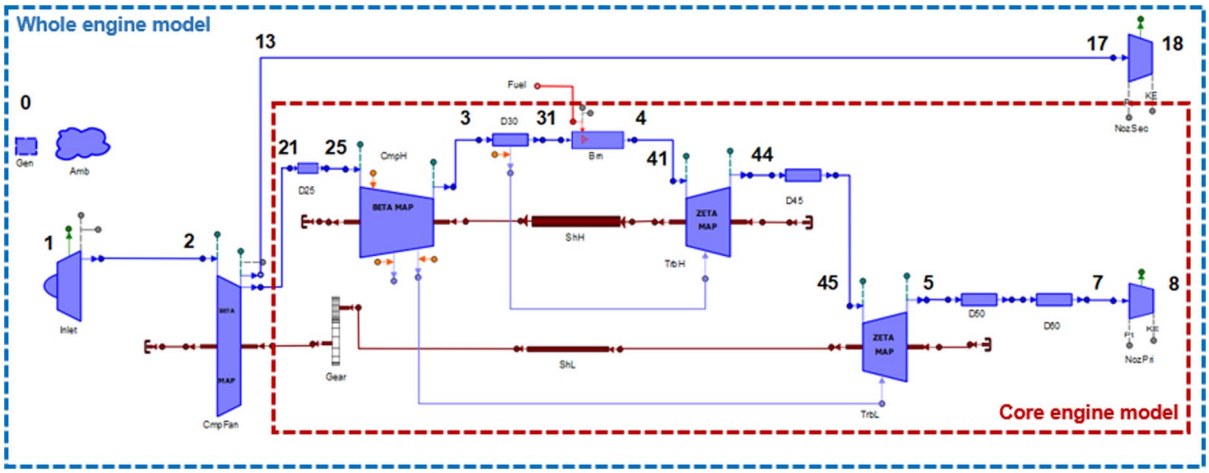

Fig. 2 Performance model of the DGEN380 turbofan.

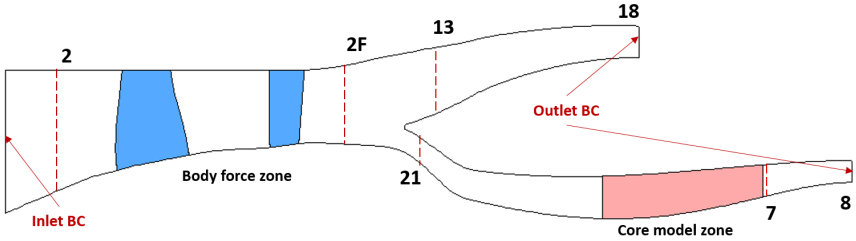

Fig. 3 Aerodynamic model of the DGEN380 turbofan (BC = Boundary Condition).

boundary condition-based coupling strategies have been showed to raise convergence challenges from the overall CFD–engine performance perspective [20,30]. In this context, the source term model is intended to make the coupling approach as seamless as possible by providing a means to naturally establish the adequate core mass flow from the total conditions at station 7 and the fuel injection. Besides, the local formulation of the source terms allows us to reach such conditions without introducing flow discontinuities in the CFD simulation, thus ensuring the global robustness of the coupling approach.

3. Governing Equations

The body force and core source term models are included in the Reynolds-averaged Navier–Stokes (RANS) equations by means of right hand-side terms (viscous and heat transfer terms are omitted for clarity),

$$\frac{\partial \boldsymbol{M}}{\partial t} + \nabla \cdot (\boldsymbol{MV}) = \nabla \cdot \boldsymbol{N} + \boldsymbol{F} \tag{1}$$

where

$$\boldsymbol{M} = \begin{bmatrix} \rho \\ \rho \boldsymbol{V} \\ \rho(e + V^2) \end{bmatrix}, \qquad \boldsymbol{N} = \begin{bmatrix} \boldsymbol{0} \\ -p\boldsymbol{I} \\ -p\boldsymbol{V} \end{bmatrix} \tag{2}$$

and $\boldsymbol{F}$ stands for a source term field. In the body force zone displayed in Fig. 3, this field corresponds to the body force model terms F_{BF}, whereas a different source term field F_{CST} is applied in the core model zone. The expressions for these fields read

$$\boldsymbol{F}_{\mathrm{BF}} = \begin{bmatrix} -\frac{1}{b}(\rho \boldsymbol{V} \cdot \nabla b) \\ -\frac{1}{b}(\rho \boldsymbol{V} \cdot \nabla b)\boldsymbol{V} + \rho \boldsymbol{f} \\ -\frac{1}{b}(\rho \boldsymbol{V} \cdot \nabla b) h_t + \rho f_\theta N r \end{bmatrix},$$

$$\boldsymbol{F}_{\mathrm{CST}} = \begin{bmatrix} \frac{W_F}{\Omega} \\ \frac{W_F}{\Omega} \cdot \boldsymbol{V} + \rho f_p^c \cdot \boldsymbol{V}/V \\ \frac{W_F}{\Omega} \cdot h_t + \rho f_p^c \cdot V + Q \end{bmatrix} \tag{3}$$

In the body force model, b is the metal blockage, and $\boldsymbol{f}$ is the force field representing the blade effects. A detailed description of both terms is out of the scope of this contribution and can be found in [14].

Regarding the core source term model, the term W_F/Ω accounts for the fuel mass flow addition with Ω being the volume in which the core source terms are applied. The scalar f_p^c acting in the momentum and energy equations is a force parallel to the local velocity vector that introduces a total pressure and total temperature rise. Finally, the term Q in the energy equation accounts for a complementary total temperature increase. The relations for f_p^c and Q on the local flow variables are derived from Hooke's law and dimensional analysis,

$$f_p^c = \frac{K_p}{\rho \mathcal{L}}(p_{t7} - p_{t7}^*) \tag{4}$$

$$Q = \rho C_p \frac{K_q}{\mathcal{L}}(T_{t7} - T_{t7}^*)V \tag{5}$$

where the values of p_{t7}^* and T_{t7}^* are the target values of total conditions at station 7 obtained from the 0D thermodynamic cycle simulation and constitute the source term model inputs. The nondimensional coefficients K_p and K_q are constants that control the response of the model to the local flow conditions with a typical value between 5.0 and 10.0, and $\mathcal{L}$ is the characteristic length of the core duct.

D. Numerical Aspects and Error Discussion

1. Numerical Settings

The CFD simulations of the present contribution are carried out using an implicit pseudotime marching scheme to reach the steady-state solution, along with a V-cycle multigrid technique for convergence acceleration. Convective fluxes are treated using a second-order Roe scheme with the Van-Albada limiter. Turbulence closure is achieved using the Spalart–Allmaras model.

2. Numerical Error Assessment for Fan Body Force Calculations

To ensure that the fan body force calculations are grid independent, a mesh refinement study is conducted for axisymmetric inflow conditions. Three meridional resolutions are used, consisting of 11,396, 45,456, and 180,928 cells, respectively. These resolutions correspond to a uniform refinement factor of 2 in both the radial and axial directions. The resolution in the circumferential direction is kept constant because it is irrelevant for performing axisymmetric inflow computations due to the local axisymmetry assumption of the body force modeling approach [14,24,31]. Following standard procedures [32,33], the Richardson extrapolation is used to compute the estimated error on each grid, as well as the observed order of accuracy. Figure 4 shows the estimated numerical error as a function of grid size, in log–log scale. The reference second-order slope is also indicated for reference, showing that the observed order of accuracy is slightly below the theoretical order, as expected for practical applications on a nonuniform mesh. The mesh retained for the rest of the Paper is the intermediate grid level, which is associated with an estimated numerical error of about 0.05%, deemed accurate enough for the present Paper.

3. Modeling Error Assessment for Fan Body Force Calculations

Body force predictions of isolated fan performance for various speed lines are compared to mixing-plane results in Fig. 5, showing the capability of the model to reproduce conventional calculations. In particular, the total pressure ratio and the isentropic efficiency in the bypass section are predicted within 0.2% and 0.2 points agreement, respectively, for the fan operating conditions encountered in the present Paper.

4. Core Source Term Model Assessment

Contrary to the fan body force model, the core model does not aim to produce a detailed physical flowfield but rather to ensure that correct total conditions are obtained at the entry of the core nozzle. For this reason, explicitly discussing numerical or modeling error is not relevant. The correct measure of the error associated to the core model is its ability to yield target values, which can be assessed independently of the implementation in the coupled model. In this respect, specific

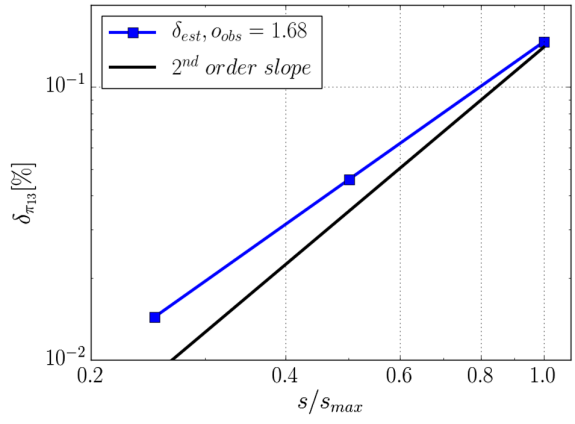

Fig. 4 Relative numerical error estimated by the Richardson extrapolation for the bypass pressure ratio.

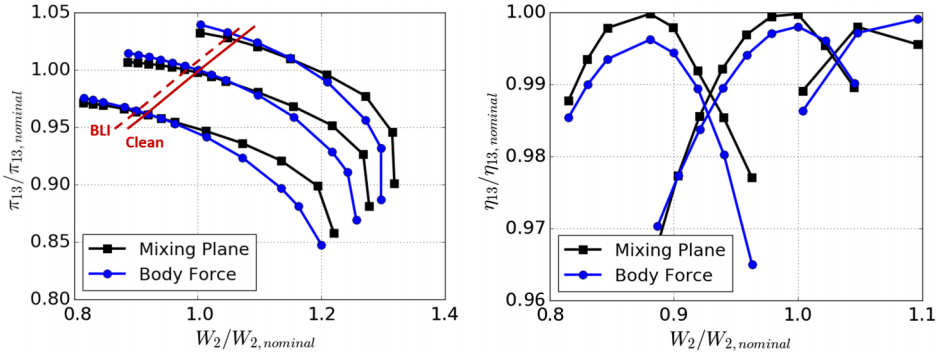

Fig. 5 Comparison of the fan body force model performance predictions against mixing-plane calculation results. The fan operating lines under clean and BLI inflow conditions are marked in red.

tests have been done using $K_p = 10$ and $K_q = 6$, which are the same values as used for the calculations presented in Sec. III. The results show that the core source term model can reproduce target values of total pressure and temperature within 0.01 and 0.003%, respectively. It should be emphasized that this ability is not dependent on the core inlet conditions, as the source term will drive the outflow to the specified target values regardless of the inflow values.

E. Coupling Implementation

The coupling between the CFD simulation and the core performance model is implemented in the FlowSimulator environment [25]. The elsA CFD solver [34] and external Python-based modules for the body force and core source term models are coupled in memory with a precompiled deck containing the PROOSIS-based performance model. A Python wrapper handles the information exchange between the CFD solver, the deck containing the core 0D model and the external modules containing the body force and core source term models. In addition, integrated tools based on the Antares Python library [35] are used to compute averaged values of the flow variables required by the performance model. In particular, stagnation quantities are mass averaged [36] and used to compute derived variables such as fan power and spool torque. This coupling process is depicted in Fig. 6 and is driven externally by setting the flight conditions h, M, and ΔT_{ISA} and the engine throttle setting through the fuel flow rate W_F.

During a coupled simulation, the 3D flowfield obtained from the CFD computation is coprocessed every 400 iterations to obtain the 0D values of core inlet total conditions and low-pressure spool torque required by the performance model to calculate the core operating point. Resulting values of low-pressure spool speed and total conditions in the primary nozzle plus fuel mass flow are used to update both the body force and the core source term models. Typically, around ten updates are sufficient for the CFD simulation to provide a converged solution in which the fan power calculated by the body force model is balanced by the low-pressure spool power predicted by the thermodynamic cycle simulation. As discussed in Sec. II.C, the updates only affect the aerodynamic model inputs, while the CFD boundary conditions remain unchanged during the whole simulation. This last point constitutes a major difference with respect to previous zooming approaches [20,22].

F. Engine Performance Metric Definition

Engine performance parameters are computed using averaged values of the CFD simulation. In particular, the computation of the net thrust and engine power must account for the engine inlet velocity, whose definition is ambiguous here as the engine external aerodynamic flow is not simulated. In this contribution, an equivalent engine inlet velocity V_0 is derived from station 2 conditions assuming that the stream tube entering the engine follows an isentropic transformation from ambient conditions to this station (i.e., $p_{t0} = p_{t2}$, $T_{t0} = T_{t2}$ and $p_0 = p_\infty$):

$$V_0 = a_0 \cdot M_0 \tag{6}$$

Engine net thrust, mechanical power, and thrust specific fuel consumption (TSFC) are then defined as in Eqs. (7), (8), and (9), respectively. Note that, because the DGEN380 nozzles operate in subsonic regime for the considered operating conditions, the pressure terms cancel and therefore are omitted for clarity in the expressions of thrust and mechanical power:

$$F_n = W_{18}V_{18} + W_8V_8 - W_2V_0 \tag{7}$$

$$P = \left(W_{18}\frac{V_{18}^2}{2} + W_8\frac{V_8^2}{2}\right) - W_2\frac{V_0^2}{2} \tag{8}$$

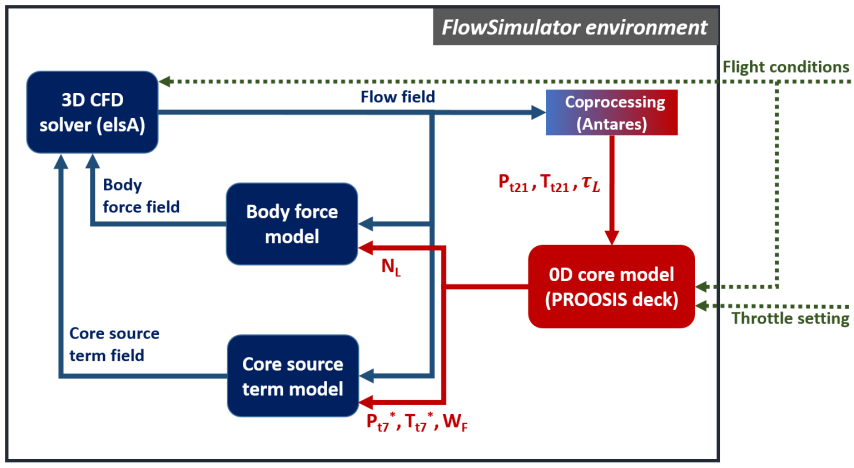

Fig. 6 Coupling implementation in the FlowSimulator environment.

$$\mathrm{TSFC} = \frac{W_F}{F_n} \tag{9}$$

Propulsive efficiency η_{prop}, thermal efficiency η_{th}, and overall efficiency η_{ovr} are derived from the previous definitions:

$$\eta_{\mathrm{prop}} = \frac{F_n \cdot V_\infty}{P} \tag{10}$$

$$\eta_{\mathrm{th}} = \frac{P}{W_F \cdot \mathrm{LHV}} \tag{11}$$

$$\eta_{\mathrm{ovr}} = \frac{F_n \cdot V_\infty}{W_F \cdot \mathrm{LHV}} = \eta_{\mathrm{prop}} \cdot \eta_{\mathrm{th}} \tag{12}$$

III. Verification of Approach at Engine Design Point

To verify the overall accuracy of the proposed coupled approach, a comparison is performed here between 1) a 0D whole engine model and 2) the coupled model described in Fig. 6. For the latter, a single-passage version of the computational domain presented in Fig. 3 is used. The associated structured, multiblock mesh features 420,000 cells with $y^+ < 1$ at the solid wall boundaries. The comparison is done for the design point, under clean inflow conditions.

Given the discussion of errors in Sec. II.D, the numerical errors of the fan body force model and those associated to the ability of the core model to reproduce target conditions can be considered negligible (with respect to the variations to be discussed in the following). Because the fan map used in the whole engine model is derived from body force model simulations, the model error of the fan will not come into play in the verification process. However, it is acknowledged that the accuracy of the coupled approach in terms of fan performance prediction will not be better than the accuracy of the body force model (see Fig. 5). Furthermore, as the design point operation is strictly enforced in the whole engine calculation, no interpolation errors in the performance maps are involved. Therefore, the verification proposed in this section gives a direct measure of the error of the coupled approach with respect to a whole engine 0D model. In this respect, it is contended that the only direct error introduced by the coupling itself is due to the use of averaging when transmitting information from the the 3D CFD domain to the PROOSIS model.

Figure 7 presents the comparison of various performance metrics obtained by the coupled and the whole engine approaches, in the form of relative errors with respect to the whole engine model. A shift in the operating point of the fan is observed, with differences of 0.15 and 0.05% for the bypass mass flow and rotational speed, respectively. As a direct consequence, slight differences are observed in the prediction of the fan bypass and core isentropic efficiency, of around 0.3 and 0.6 points, respectively. The error introduced by the averaging process thus has a compound effect, in the sense that the core of the coupled model is subject to different conditions than in the whole engine model, leading to a very small variation of its operation, which in turn modifies the fan operating point via the coupling process, and therefore all the engine operation. From the overall performance standpoint, variations in propulsive, thermal, and overall efficiency remain inferior to 0.1 points.

To conclude the verification process, the variations between the coupled and whole engine models are small and could be viewed as inherent uncertainties when comparing the two approaches. However, this is not the case when comparing coupled simulations, as the averaging is always present.

IV. Assessment of BLI Effects

In this section, the coupled methodology is applied to a BLI configuration in order to assess the impact of inflow distortion on engine overall performance (Sec. IV.A), internal aerodynamics (Sec. IV.B), and rotordynamics (Sec. IV.C). To this end, a vertically stratified total pressure distribution with a spatial extent of 30% of the engine diameter is imposed at the inlet of a full-annulus computational domain, about one fan diameter upstream of station 2. This distortion is representative of the boundary layer that could be encountered at the rear end of a 10-m-length light jet aircraft cruising at the DGEN380 design flight conditions. As both nozzles remain unchoked for the study presented here, static pressure outflow boundary conditions are set at the domain outlet (sections 8 and 18). The associated structured, multiblock mesh features around 25 million cells with $y^+ < 1$ at the solid wall boundaries. The effects of this distortion are explored for the altitude and Mach number displayed and five levels of engine net thrust, ranging from 80 to 130% of its nominal value. For each throttle setting, engine performance is compared to the results obtained with clean inflow conditions. Figure 8 depicts a meridional view of the computational domain and illustrates how the fan body force and core source term models reproduce local aerodynamic effects of boundary layer ingestion. For each thrust setting, approximately 6 h of computational time using 120 CPUs on a High Performance Computing (HPC) cluster were necessary to reach convergence.

In this Paper, the distortion pattern is assumed to remain unchanged along the engine operating range as the airframe–engine aerodynamic interactions are not modeled. Figure 9 depicts this distortion and shows the upstream effect of the fan. Because of the low flight Mach number, the mass-averaged total pressure at the fan face drops only in about 0.4%. Nevertheless, this drop is sufficient to induce reduc-

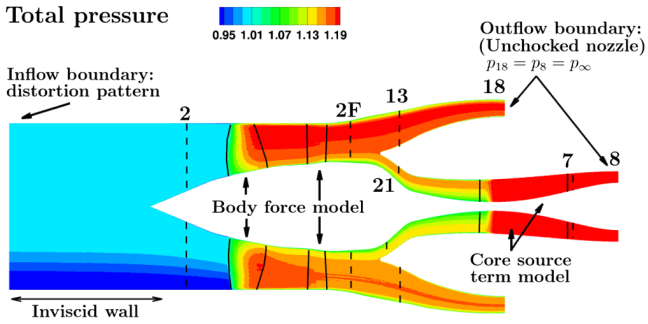

Fig. 8 Meridional view of the coupled simulation results for $F_n/F_{n,\mathrm{nom}} = 1.3$. Contours of total pressure normalized by freestream total pressure.

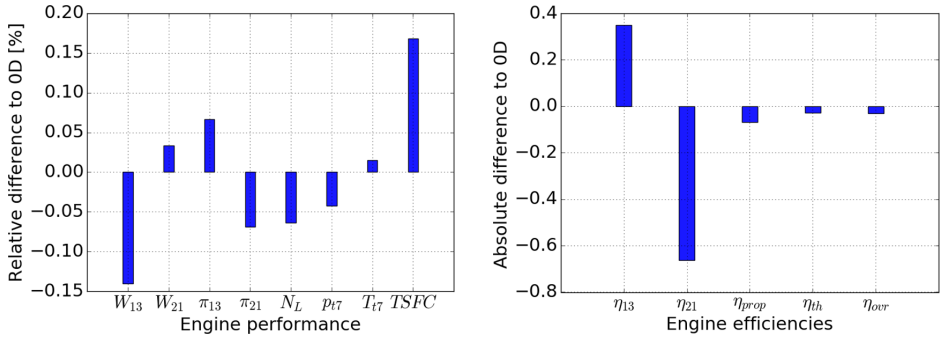

Fig. 7 Comparison of results from the performance model and the coupled simulations.

tions of the equivalent inflow velocity defined in Eq. (6) of around 2%, which is the figure that drives BLI propulsive gains [37]. Although not shown in this contribution, this order of magnitude is actually comparable to those encountered on a larger turbofan engine cruising at Mach number of 0.78. It should be emphasized here that the previously mentioned hypothesis must be kept in mind when interpreting the evolution of Fig. 9, as in a full aircraft configuration the capture area could vary with modifications in thrust, thus altering the relative amount of low momentum fluid ingested. In any case, the application of the present methodology to aircraft–engine configurations is straightforward, because only an adaptation of the computational domain to include the airframe would be required.

A. BLI Impact on Overall Engine Performance

Figure 10 shows the impacts of boundary layer ingestion on fan performance. As depicted in the left-hand side plot, a shift is induced in the fan operating point. In particular, the combination of the inflow-corrected mass flow drop of around 0.7% and the potential negative effects of inflow distortion in fan stability limits results in a reduction of the fan surge margin. The right-hand side plot illustrates the isentropic efficiency penalty along the whole span as measured in the bypass duct (station 13) and core inlet (station 21). This penalty is more pronounced in the bypass duct, where the efficiency drops about 0.8 points for all the thrust settings considered.

Figure 11 provides an assessment of BLI benefits in terms of engine efficiencies, mechanical power and TSFC. The fan efficiency drop is partially responsible for the thermal efficiency decrease, estimated to be around 0.1 points. On the other hand, the reduction of inflow velocity provides a gain in propulsive efficiency: less power is required to produce a given net thrust when slow-moving fluid is accelerated, instead of freestream air. Furthermore, in the present case, the lower inflow velocity is sufficient to allow the bypass exhaust velocity to remain essentially unaltered for reaching constant thrust, while it compensates the mass flow reduction through the engine induced by the ingestion of the boundary layer. Quantitatively, these effects translate into a reduction of mechanical power in about 1%, equivalent to a 0.6 point gain in propulsive efficiency in the present case. Altogether, the opposite effects of BLI in thermal and propulsive efficiency lead to a 0.1 point gain for the overall efficiency, which provides a 0.7% reduction in TSFC.

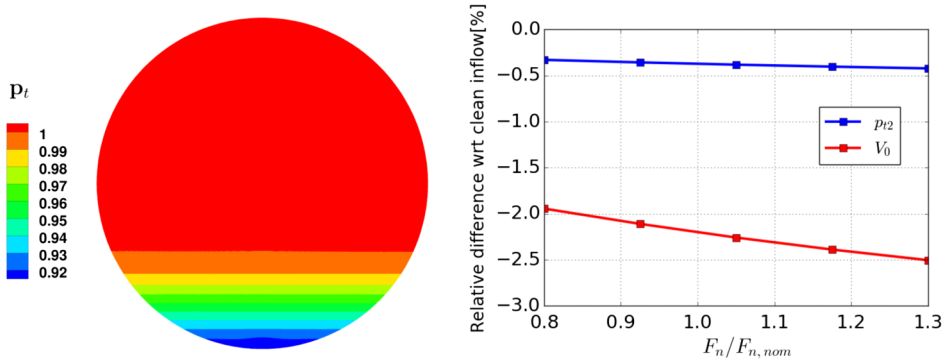

Fig. 9 Inlet distortion profile and induced inflow velocity and mass-averaged total pressure drops as compared to clean inflow operation.

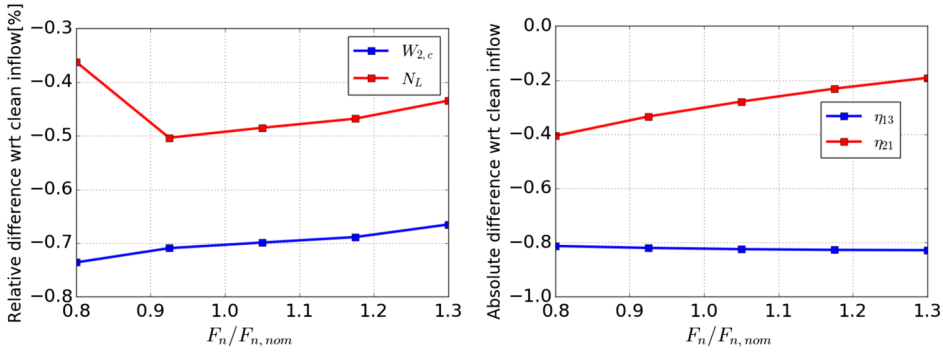

Fig. 10 BLI effect on fan operation.

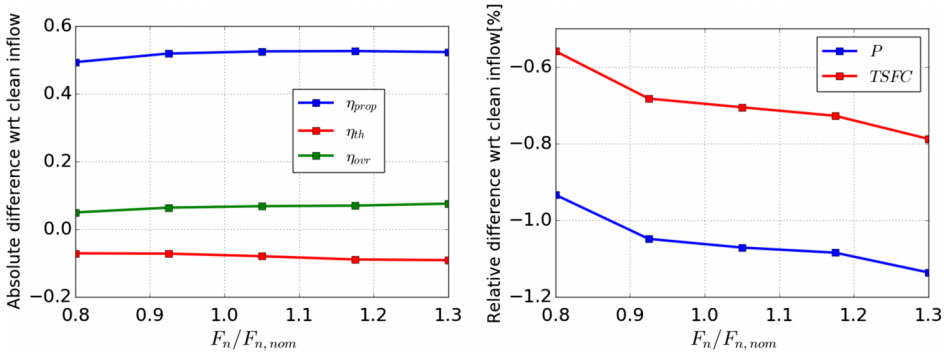

Fig. 11 BLI effect on engine performance.

Overall, for a fixed engine net thrust requirement, the impact of this boundary layer inflow configuration on global engine performance is not significant as the gains remain relatively small. In a more general scenario, two additional considerations must be taken into account. On the one hand, propulsion–airframe integration effects have been demonstrated to further enhance the BLI benefits [4,5], due to the reduction of flight power requirement for a given cruise condition. On the other hand, the figures obtained in this Paper should not be extrapolated to engines cruising at higher Mach numbers. Although gains in propulsive efficiency might be similar due to comparable reductions of engine inflow velocity, the higher total pressure distortion levels expected for such flight conditions imply larger fan isentropic efficiency penalties, which would lower or potentially suppress the overall benefits.

B. BLI Impact on Fan Stage Aerodynamics

As investigated by Gunn and Hall [11], the coswirling and counterswirling regions induced upstream of the rotor section due to flow migration around the spinner, together with the local deficit in axial velocity, generate an inhomogeneous work input around the annulus. Additionally, off-design blade incidences trigger locally increased losses. Figure 12 provides an investigation of these phenomena for the thrust setting $F_n/F_{n,\mathrm{nom}} = 1.3$. In the coswirling region, the fan imparts less work because of the positive tangential component of the inlet absolute velocity. The inverse is true for the counterswirling region, where more work is added. These observations are confirmed through the comparison of spanwise profiles of total pressure ratio at three different circumferential locations, obtained by applying streamlining procedures to match the positions of the particles lying at $\theta = 90$ deg (a), $\theta = 210$ deg (b), and $\theta = 330$ deg (c) at station 2 to their final position at station 2F. The profiles of isentropic efficiency also show important variations, which are more noticeable in the near-tip spans of the counterswirling region.

As a result of the previous mechanisms, the total pressure pattern is modified and convected through the fan stage. Figures 13 and 14 display the contours of this variable at the bypass duct (section 13) and core inlet (section 21) for the lowest, medium, and highest thrust settings. At section 21, an important consequence of the swirling flow at the fan face is noticed. In spite of the small portion of ingested low-momentum fluid, the core section presents a nonuniform total pressure field in the circumferential direction. Similarly, the static pressure field features a circumferential distortion, although to a much lesser extent than the total pressure. Two conclusions are drawn from these observations. On the one hand, accounting for the three-dimensional nature of the fan–distortion interaction becomes essential for the prediction of BLI performance. Although the impacts for the studied case are not significant, core inflow distortion could imply negative consequences on core component efficiency, which translates into an increased thermal efficiency penalty, and core operability, such as surge margin reduction in compressors, potentially outweighing aerodynamic benefits. Accurately capturing the 3D flow field features thus becomes essential to quantify such phenomena, which cannot be achieved through thermodynamic cycle simulations only. On the other hand, the use of the core source term model presents an advantage with respect to a boundary condition-based approach for configurations with nonnegligible levels of static pressure distortion, because it allows this variable to be a result of the fan stage aerodynamics rather than a prescribed distribution

C. BLI Impact on Rotordynamics

Besides performance and aerodynamic effects, BLI raises aeromechanical challenges. In particular, inlet distortion induces an unsteady

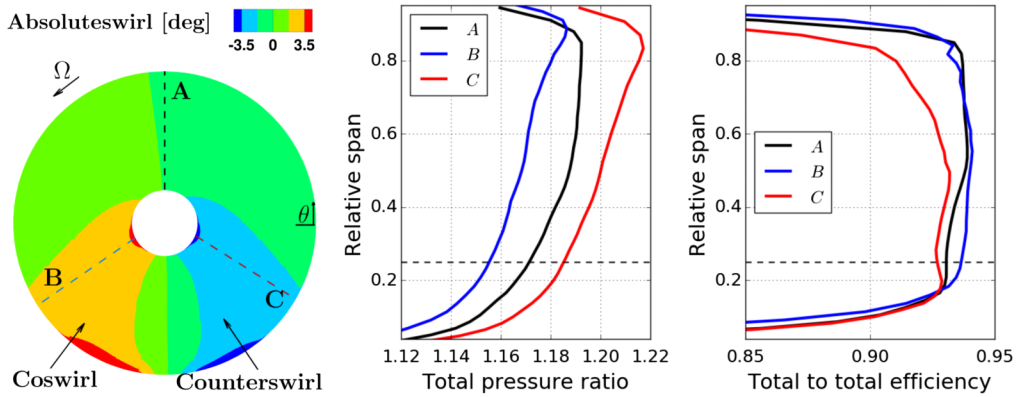

Fig. 12 Absolute swirl angle at station 2 induced by the fan upstream effect (left) and variations in rotor total pressure ratio and isentropic efficiency profiles around the annulus (right), with the position of the splitter marked with a dashed line.

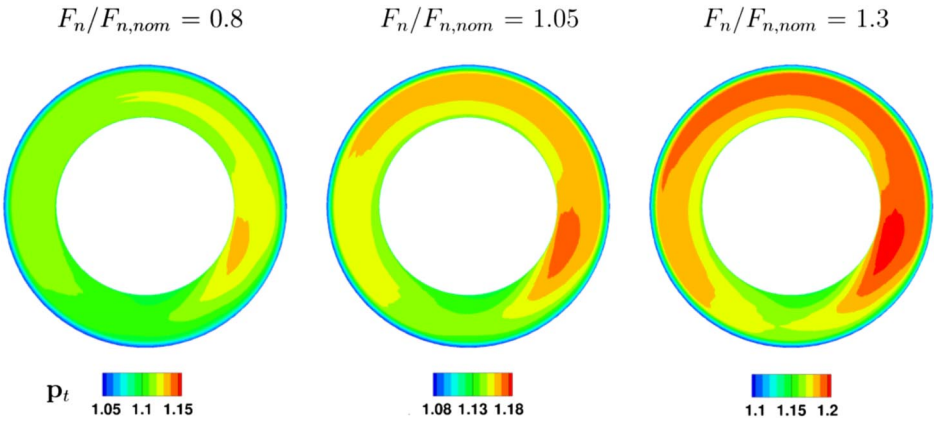

Fig. 13 Contours of total pressure at station 13. Values normalized with freestream total pressure.

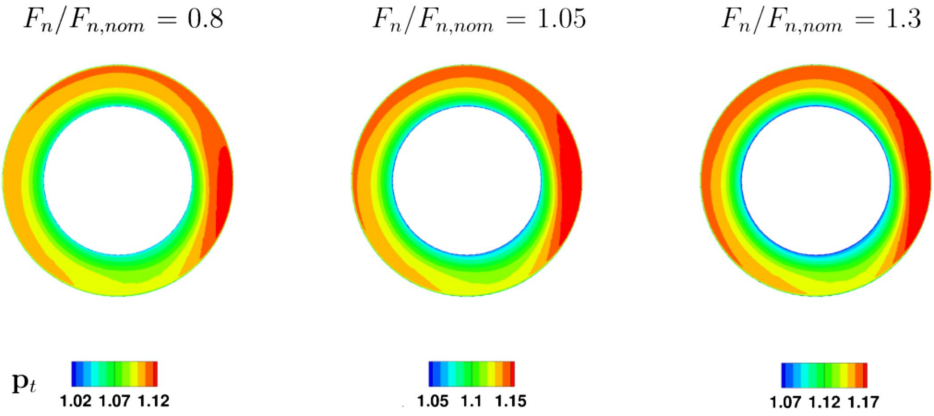

Fig. 14 Contours of total pressure at station 21. Values normalized with freestream total pressure.

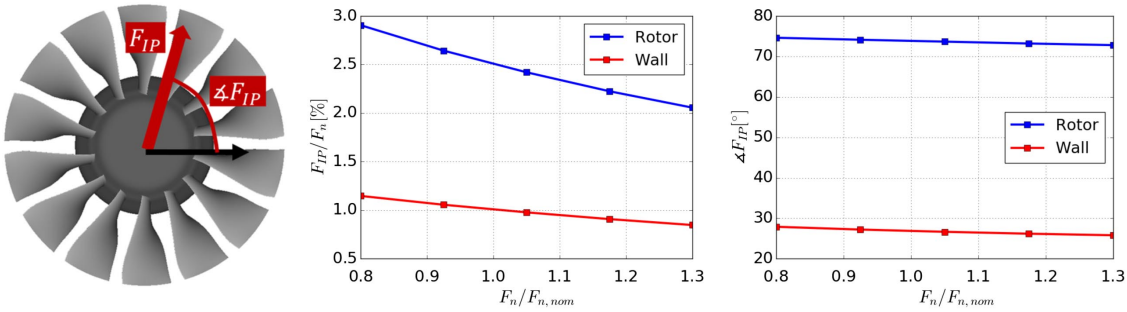

Fig. 15 In-plane force definition (left) and evolution of the modulus and phase of the rotor blades and fan stage wall contributions (right).

blade loading characterized by a once-per-revolution frequency. Although the steady nature of the body force modeling approach cannot capture such a time-dependent phenomenon, the integration of the force field in the bladed region yields the steady component of resultant force in the plane orthogonal to the rotation axis due to the nonuniform blade loading around the annulus. In addition, the non-axisymmetric pressure and viscous stress distribution on the spinner and fan stage hub contribute to this resultant force. This solicitation is known as in-plane force and is characterized by its modulus and phase, as conceptually depicted in the left-hand side of Fig. 15. The prediction of the in-plane force is of particular importance for rotordynamics, as this load must be withstood by the fan spool.

The left-hand side plot of Fig. 15 characterizes the rotor loading and the wall pressure, referred to as p_∞ because the integral is calculated on a nonclosed surface, and viscous stress contributions to the in-plane force modulus, as a function of the thrust setting. For the rotor loading, the resultant force ranges between 2 and 3% of the net thrust. Results indicate that the contribution of the spinner and hub to the in-plane force are nonnegligible and represent around 1% of the net thrust. The phase remains unaltered by the thrust setting. For the rotor, results indicate that the in-plane force is close to be vertical. Conversely, the wall in-plane force appears to be almost horizontal.

V. Conclusions

In this contribution, a coupled body force–engine performance approach has been introduced to simultaneously predict fan stage aerodynamics and overall engine performance in BLI configurations. The methodology is based on a reduced-order representation of the engine internal aerodynamics using the body force technique, coupled with a thermodynamic cycle model to account for core performance. Fundamental advantages of this approach include its capability to provide a multifidelity assessment of the engine behavior at an affordable computational cost, its suitability to be applied to CFD computations of airframe–engine configurations, and the possibility to drive the coupling by specifying only one engine performance parameter.

The coupled approach has been verified against reference thermodynamic cycle calculations and subsequently demonstrated in the assessment of BLI impacts on the DGEN380 turbofan operation for several thrust settings. Engine performance results highlight that, although fan efficiency is penalized and surge margin is decreased, small benefits in mechanical power and thrust specific fuel consumption for a given net thrust level can be achieved. Three-dimensional fan stage flow analysis reveals that the flow distortion transfer mechanisms induced by the fan–distortion aerodynamic interaction are responsible for core inlet distortion, which might have negative consequences in thermal efficiency and core operability.

Future work will focus on applying this approach to investigate the potential gains of BLI in aircraft–engine configurations, thus accounting for the aerodynamic coupling effects between the engine and the airframe.

Acknowledgment

Airbus is gratefully acknowledged for the support provided during this study.

References

[1] Smith, L. H., "Wake Ingestion Propulsion Benefit," *Journal of Propulsion and Power*, Vol. 9, No. 1, 1993, pp. 74–82. https://doi.org/10.2514/3.11487

[2] Drela, M., "Power Balance in Aerodynamic Flows," *AIAA Journal*, Vol. 47, No. 7, 2009, pp. 1761–1771. https://doi.org/10.2514/1.42409

[3] Florea, R. V., Matalanis, C., Hardin, L. W., Stucky, M., and Shabbir, A., "Parametric Analysis and Design for Embedded Engine Inlets," *Journal of Propulsion and Power*, Vol. 31, No. 3, 2015, pp. 843–850. https://doi.org/10.2514/1.B34804

[4] Hall, D. K., Huang, A. C., Uranga, A., Greitzer, E. M., Drela, M., and Sato, S., "Boundary Layer Ingestion Propulsion Benefit for Transport Aircraft," *Journal of Propulsion and Power*, Vol. 33, No. 5, 2017, pp. 1118–1129. https://doi.org/10.2514/1.B36321

[5] Uranga, A., Drela, M., Greitzer, E. M., Hall, D. K., Titchener, N. A., Lieu, M. K., Siu, N. M., Casses, C., Huang, A. C., Gatlin, G. M., and Hannon, J. A., "Boundary Layer Ingestion Benefit of the D8 Transport Aircraft," *AIAA Journal*, Vol. 55, No. 11, 2017, pp. 3693–3708. https://doi.org/10.2514/1.J055755

[6] Liu, C., Doulgeris, G., Laskaridis, P., and Singh, R., "Thermal Cycle Analysis of Turboelectric Distributed Propulsion System with Boundary Layer Ingestion," *Aerospace Science and Technology*, Vol. 27, No. 1, 2013, pp. 163–170. https://doi.org/10.1016/j.ast.2012.08.003

[7] Dae Kim, H., Felder, J. L., Tong, M. T., Berton, J. J., and Haller, W. J., "Turboelectric Distributed Propulsion Benefits on the N3-X Vehicle," *Aircraft Engineering and Aerospace Technology*, Vol. 86, No. 6, 2014, pp. 558–561. https://doi.org/10.1108/AEAT-04-2014-0037

[8] Kirner, R., Raffaelli, L., Rolt, A., Laskaridis, P., Doulgeris, G., and Singh, R., "An Assessment of Distributed Propulsion: Advanced Propulsion System Architectures for Conventional Aircraft Configurations," *Aerospace Science and Technology*, Vol. 46, Oct. 2015, pp. 42–50. https://doi.org/10.1016/j.ast.2015.06.022

[9] Gray, J. S., Mader, C. A., Kenway, G. K., and Martins, J. R., "Modeling Boundary Layer Ingestion Using a Coupled Aeropropulsive Analysis," *Journal of Aircraft*, Vol. 55, No. 3, 2018, pp. 1191–1199. https://doi.org/10.2514/1.C034601

[10] Fidalgo, V. J., Hall, C., and Colin, Y., "A Study of Fan-Distortion Interaction Within the NASA Rotor 67 Transonic Stage," *Journal of Turbomachinery*, Vol. 134, No. 5, 2012, Paper 051011. https://doi.org/10.1115/1.4003850

[11] Gunn, E. J., and Hall, C., "Aerodynamics of Boundary Layer Ingesting Fans," *Proceedings of the ASME Turbo Expo 2014: Turbine Technical Conference and Exposition*, American Soc. of Mechanical Engineers, Vol. 1A, 2014, p. V01AT01A024. https://doi.org/10.1115/GT2014-26142

[12] Carrier, G., Atinault, O., Grenon, R., and Verbecke, C., "Numerical and Experimental Aerodynamic Investigations of Boundary Layer Ingestion for Improving Propulsion Efficiency of Future Air Transport," *31st AIAA Applied Aerodynamics Conference*, AIAA Paper 2013-2406, 2013.

[13] Blumenthal, B. T., Elmiligui, A. A., Geiselhart, K. A., Campbell, R. L., Maughmer, M. D., and Schmitz, S., "Computational Investigation of a Boundary-Layer-Ingestion Propulsion System," *Journal of Aircraft*, Vol. 55, No. 3, 2018, pp. 1141–1153. https://doi.org/10.2514/1.C034454

[14] Thollet, W., Dufour, G., Carbonneau, X., and Blanc, F., "Body-Force Modeling for Aerodynamic Analysis of Air Intake–Fan Interactions," *International Journal of Numerical Methods for Heat & Fluid Flow*, Vol. 26, No. 7, 2016, pp. 2048–2065. https://doi.org/10.1108/HFF-07-2015-0274

[15] Hall, D., Greitzer, E., and Tan, C., "Analysis of Fan Stage Conceptual Design Attributes for Boundary Layer Ingestion," *Journal of Turbomachinery*, Vol. 139, No. 7, 2017, Paper 071012. https://doi.org/10.1115/1.4035631

[16] Cao, T., Hield, P., and Tucker, P. G., "Hierarchical Immersed Boundary Method with Smeared Geometry," *Journal of Propulsion and Power*, Vol. 33, No. 5, 2017, pp. 1151–1163. https://doi.org/10.2514/1.B36190

[17] Follen, G., and AuBuchon, M., "Numerical Zooming Between a NPSS Engine System Simulation and a One-Dimensional High Compressor Analysis Code," NASA TM-209913, 2000. https://doi.org/10.1.1.114.6728

[18] Turner, M. G., Reed, J. A., Ryder, R., and Veres, J. P., "Multi-Fidelity Simulation of a Turbofan Engine with Results Zoomed into Mini-Maps for a Zero-D Cycle Simulation," *Proceedings of the ASME Turbo Expo 2004: Power for Land, Sea, and Air*, Vol. 2, American Soc. of Mechanical Engineers, Vienna, Austria, June 2004, pp. 219–230. https://doi.org/10.1115/GT2004-53956

[19] Klein, C., Reitenbach, S., Schoenweitz, D., and Wolters, F., "A Fully Coupled Approach for the Integration of 3D-CFD Component Simulation in Overall Engine Performance Analysis," *Proceedings of the ASME Turbo Expo 2017: Turbomachinery Technical Conference and Exposition*, Vol. 1, American Soc. of Mechanical Engineers, Charlotte, North Carolina, June 2017, Paper V001T01A014. https://doi.org/10.1115/GT2017-63591

[20] Pachidis, V., Pilidis, P., Talhouarn, F., Kalfas, A., and Templalexis, I., "A Fully Integrated Approach to Component Zooming Using Computational Fluid Dynamics," *Journal of Engineering for Gas Turbines and Power*, Vol. 128, No. 3, 2006, pp. 579–584. https://doi.org/10.1115/1.2135815

[21] Pachidis, V., Pilidis, P., Marinai, L., and Templalexis, I., "Towards a Full Two Dimensional Gas Turbine Performance Simulator," *Aeronautical Journal*, Vol. 111, No. 1121, 2007, pp. 433–442. https://doi.org/10.1017/S0001924000004693

[22] Pilet, J., Lecordix, J. L., Garcia-Rosa, N., Barènes, R., and Lavergne, G., "Towards a Fully Coupled Component Zooming Approach in Engine Performance Simulation," *Proceedings of the ASME 2011 Turbo Expo: Turbine Technical Conference and Exposition*, Vol. 1, American Soc. of Mechanical Engineers, Vancouver, British Columbia, Canada, June 2011, pp. 287–299. https://doi.org/10.1115/GT2011-46320

[23] Alexiou, A., Baalbergen, E., Kogenhop, O., Mathioudakis, K., and Arendsen, P., "Advanced Capabilities for Gas Turbine Engine Performance Simulations," *ASME Turbo Expo 2007: Power for Land, Sea, and Air*, American Soc. of Mechanical Engineers, Fairfield, NJ, 2007, pp. 19–28.

[24] Peters, A., Spakovszky, Z. S., Lord, W. K., and Rose, B., "Ultrashort Nacelles for Low Fan Pressure Ratio Propulsors," *Journal of Turbomachinery*, Vol. 137, No. 2, 2015, Paper 021001. https://doi.org/10.1115/1.4028235

[25] Meinel, M., and Einarsson, G. O., "The FlowSimulator Framework for Massively Parallel CFD Applications," *PARA 2010 Conference: State of the Art in Scientific and Parallel Computing*, 2010. https://doi.org/10.1.1.458.3389

[26] Garcia Rosa, N., Dufour, G., Barènes, R., and Lavergne, G., "Experimental Analysis of the Global Performance and the Flow Through a High-Bypass Turbofan in Windmilling Conditions," *Journal of Turbomachinery*, Vol. 137, No. 5, 2015, Paper 051001. https://doi.org/10.1115/1.4028647

[27] Culmone, M. V., Garcia-Rosa, N., and Carbonneau, X., "Sensitivity Analysis and Experimental Validation of Transient Performance Predictions for a Short-Range Turbofan," *ASME Turbo Expo 2016: Turbomachinery Technical Conference and Exposition*, American Soc. of Mechanical Engineers Digital Collection, Vol. 1, Fairfield, NJ, June 2016. https://doi.org/10.1115/GT2016-57257

[28] Stabe, R., Whitney, W., and Moffitt, T., "Performance of a High-Work Low Aspect Ratio Turbine Tested with a Tealistic Inlet Tadial Temperature Profile," *20th Joint Propulsion Conference*, AIAA Paper 1984-1161, 1984. https://doi.org/10.2514/6.1984-1161

[29] Sethi, V., Doulgeris, G., Pilidis, P., Nind, A., Doussinault, M., Cobas, P., and Rueda, A., "The Map Fitting Tool Methodology: Gas Turbine Compressor Off-Design Performance Modeling," *Journal of Turbomachinery*, Vol. 135, No. 6, 2013, Paper 061010. https://doi.org/10.1115/1.4023903

[30] Pilet, J., "Analyse du Comportement Moteur Stabilisé en Windmilling par Couplage des Modèles Thermodynamiques et Simulations Numériques," Ph.D. Thesis, ISAE-SUPAERO, Univ. of Toulouse, Toulouse, France, 2013.

[31] Hall, D., Greitzer, E., and Tan, C., "Analysis of Fan Stage Design Attributes for Boundary Layer Ingestion," *ASME Turbo Expo 2016: Turbomachinery Technical Conference and Exposition*, American Soc. of Mechanical Engineers, Fairfield, NJ, 2016, p. V02AT37A047.

[32] Roache, P. J., "Verification of Codes and Calculations," *AIAA Journal*, Vol. 36, No. 5, 1998, pp. 696–702. https://doi.org/10.2514/2.457

[33] Celik, I. B., and Li, J., "Assessment of Numerical Uncertainty for the Calculations of Turbulent Flow over a Backward-Facing Step," *International Journal for Numerical Methods in Fluids*, Vol. 49, No. 9, 2005, pp. 1015–1031. https://doi.org/10.1002/fld.1040

[34] Cambier, L., Heib, S., and Plot, S., "The Onera elsA CFD Software: Input from Research and Feedback from Industry," *Mechanics & Industry*, Vol. 14, No. 3, 2013, pp. 159–174. https://doi.org/10.1051/meca/2013056

[35] Gomar, T., and Léonard, T., "Antares: Python Post-Processing Library," European Center for Research and Advanced Training in Scientific Computing, 2012.

[36] Cumpsty, N., and Horlock, J., "Averaging Nonuniform Flow for a Purpose," *Journal of Turbomachinery*, Vol. 128, No. 1, 2006, pp. 120–129. https://doi.org/10.1115/1.2098807

[37] Gearhart, W. S., and Henderson, R. E., "Selection of a Propulsor for a Submersible System," *Journal of Aircraft*, Vol. 3, No. 1, 1966, pp. 84–90. https://doi.org/10.2514/3.59270

T. J. Praisner
Associate Editor